Wang *et al.*
Chinese Journal of Mechanical Engineering (2023) 36:106
https://doi.org/10.1186/s10033-023-00912-7

Chinese Journal of Mechanical Engineering

ORIGINAL ARTICLE

Open Access

Multiscale Evaluation of Mechanical Properties for Metal-Coated Lattice Structures

Lizhe Wang[1,2], Liu He[3], Xiang Wang[1,2], Sina Soleimanian[1,2], Yanqing Yu[3], Geng Chen[4*], Ji Li[3] and Min Chen[1*]

Abstract

With the combination of 3D printing and electroplating technique, metal-coated resin lattice is a viable way to achieve lightweight design with desirable responses. However, due to high structural complexity, mechanical analysis of the macroscopic lattice structure demands high experimental or numerical costs. To efficiently investigate the mechanical behaviors of such structure, in this paper a multiscale numerical method is proposed to study the effective properties of the metal-coated Body-Centered-Cubic (BCC) lattices. Unlike studies of a similar kind in which the effective parameters can be predicted from a single unit cell model, it is noticed that the size effect of representative volume element (RVE) is severe and an insensitive prediction can be only obtained from models containing multiple-unit-cells. To this end, the paper determines the minimum number of unit cells in single RVE. Based on the proposed method that is validated through the experimental comparison, parametric studies are conducted to estimate the impact of strut diameter and coating film thickness on structural responses. It is shown that the increase of volume fraction may improve the elastic modulus and specific modulus remarkably. In contrast, the increase of thickness of coating film only leads to monotonously increased elastic modulus. For this reason, there should be an optimal coating film thickness for the specific modulus of the lattice structure. This work provides an effective method for evaluating structural mechanical properties via the mesoscopic model.

Keywords Metal-coated lattice, Homogenization theory, Parametric study, Elastic and specific modulus

1 Introduction

Engineers were interested to lighten the weight of industrial components by creating perforations for decades [1–3]. The idea of making perforations was developed lattice structure concept, which offers very promising applications nowadays. Lattices keep the material only in necessary directions and critical zones, which can reduce the weight of the structure effectively [4]. To manufacture lattice structures, CNC milling machines were used to make appropriate cutouts but it limited to simple geometries and size scales [5]. In recent years, the development of Additive Manufacturing (AM) greatly has enriched the diversity of lattice design [6] providing the possibility to fabricate complex lattice components with uniform properties through a highly automated process [7, 8].

The input material properties for 3D printing process can be classified into metal and non-metal types. It is obvious that metal printed components overwhelm the non-metal ones in mechanical properties, yet the expense both in 3D printing machine itself and the base material is far higher than the plastic ones. However, there are still some limitations for 3D printing technique in terms of input material and desired performance for particular applications. In this regard, embedded metal coating film should be a possible

*Correspondence:
Geng Chen
gengchen@bjtu.edu.cn
Min Chen
min.chen@xjtlu.edu.cn
[1] School of Advanced Technology, Xi'an Jiaotong-Liverpool University, Suzhou 210053, China
[2] School of Engineering, University of Liverpool, Liverpool L69 3BX, UK
[3] Key Laboratory of MEMS of the Ministry of Education, Southeast University, Nanjing 210096, China
[4] School of Mechanical, Electronic and Control Engineering, Beijing Jiaotong University, Beijing 100044, China

solution which can alter the material properties for desired structural characteristics. The coating treatment may not only enhance structural stiffness and strength, but lead to super specific purposes, like resistance against elevated temperatures, contact stress concentration, surface failures, fire flame, and corrosion [9–11].

Coating of 3D printed scaffolds leads to the surface improvement which offers high cell adhesion capacity favorable for bone tissue replica [12]. Polylactic Acid (PLA) printed lattice structure coated by titanium witnessed its improved strength applicable for mandibular prosthesis. Layered coatings were recommended to be applied into lattice structures to stimulate the bone tissue behavior and improve their biocompatibility [13]. A recent study revealed 68% improvement of structural elastic modulus for Body-Centered-Cubic (BCC) lattice structure treated by coating film [14]. The general stress analyses of coated lattice structures were already studied through analytical [15], numerical [16, 17], or experimental approaches [18].

In analytical and numerical methods, lattice is treated as a special type of composites, whose equivalent properties are common to be mapped from local to global level. Multiscale evaluation of effective properties for lattice structures with narrow rods was conducted through analytical formulations in previous studies [19]. This enables the researcher to avoid high computation cost in the simulation of large-scale structures. The bridge between local and global level is the homogenization theory, which assesses the structure properties through a volumetric averaging technique and mechanics constitutive laws [19–23]. However, most previous work in this field defined the single unit cell as the Representative Volume Element (RVE) only based on the geometry compatibility, ignoring the structural impact of the unit cell.

Moreover, little research has paid attention to the numerical prediction of homogenized material properties for coated lattices [24]. The rods in the plastic lattice are usually measured in millimeters, while the coating film in a micrometer scale. The appropriate finite element definitions played an important role in the simulation [25, 26]. In addition to various design references for lattices, there are many uncertainties in the lattice printing and coating process, which involves plenty of parameters in the setting. Therefore, the central purpose of this work is to provide a reliable reference for evaluating mechanic properties of coated lattice structures through the multiscale numerical method. The BCC lattice structure was taken as an illustrative example to verify the numerical method and the rationality and precision of the proposed method were also validated by macroscopic experiments. Afterwards, factor analyses were conducted for assessing design impacts on the overall elastic performance of the coated lattice structure.

2 Multiscale Analysis of Lattice Structure

2.1 Mechanical Property Evaluation Based on the Homogenization Method

Like conventional multi-phase composite materials, it is extremely challenging to simulate structural components composed of micro/meso-scale lattices, due to the high modelling and computational cost. Based on the classical multiscale principle, the minimal repeatable structure can be defined as the RVE, which should be small enough not to be affected by larger scale parameters, simultaneously big enough to meet the research geometry parametrization requirement [27, 28].

The homogenization theory evaluates the volume weighted values for stress and strain. The core idea of this theory is that the homogenized physical properties can be interpreted as the physical parameter of the homogeneous material whose overall response is "close" to that of the heterogeneous periodic material, when the size of the cell tends to zero [20, 21]. It can be applied at micro/meso-scales satisfying the problem requirements [23, 29].

For the RVE with voids, many researchers took the effect of voids of the same size into account, although in a more complex case, two populations of voids with different sizes were studied [30]. In the present approach, the efficiency of the classic homogenization theory on prediction of effective Young's modulus (E) is investigated when the RVE includes void regions.

According to homogenization theory, the macroscopic stress $\boldsymbol{\Sigma}$ and strain E can be computed by integration over local stress $\sigma(x)$ and strain $\varepsilon(x)$ as follows:

$$\boldsymbol{\Sigma} = \frac{1}{V}\int_V \boldsymbol{\sigma}(\boldsymbol{x})\mathrm{d}V = \langle \boldsymbol{\sigma} \rangle, \tag{1}$$

$$\mathrm{E} = \frac{1}{V}\int_V \varepsilon(x)\mathrm{d}V = \langle \boldsymbol{\varepsilon} \rangle, \tag{2}$$

where $\langle \cdot \rangle$ strands for the average operator on volume domain, and V is the volume of the representative element. For lattice structure, $V = V_{\text{solid}} + V_{\text{void}}$ while the stress of the void part is zero. Introducing the fourth-order effective elastic tensor $\boldsymbol{C_{eff}}$ and from the Eq. (1) and Eq. (2), the $\boldsymbol{\Sigma}$ and E satisfies:

$$\boldsymbol{\Sigma} = \boldsymbol{C_{eff}} : \mathrm{E}. \tag{3}$$

Considering the 3D homogeneous material model and the geometrical symmetry, the BCC-like lattice RVE deforms isotopically; which means the properties are independent of direction. The typical directional Young's modulus (E_i, i=1, 2, 3) for each element can be estimated

under uniaxial loading condition in the corresponding direction, and expressed as:

$$E_1 = E_2 = E_3 = \frac{\mathbf{\Sigma}_i}{E_i}, i = 1, 2, 3. \tag{4}$$

However, for ease of estimating E without the numerical integration of $\sigma(x)$ and $\varepsilon(x)$ based on average stress-strain relations, due to the homogeneous material property and the uniaxial tensile test condition, another convenient way for the anticipation of E is utilized in this work as follows:

$$E_1 = E_2 = E_3 = \frac{\mathbf{\Sigma}_1}{E_1} = \frac{\boldsymbol{F}/A}{\boldsymbol{\delta}/L} = \frac{\boldsymbol{F}L}{\boldsymbol{\delta}A}, \tag{5}$$

where $\boldsymbol{F}$ is the uniaxial reaction force caused by the input loading, $\boldsymbol{\delta}$ is the uniaxial external displacement, L and A represent the dimension and cross-sectional area of lattice cell.

2.2 Periodic Boundary Conditions (PBCs)

With the proposed homogenization method, the RVE should satisfy periodic conditions, which indicates that the deformed RVE under imposed loads may expand compatibly in both geometric and physical fields. There are 3 approaches in the numerical implementation, the uniform strain, the uniform stress and PBCs [31]. The first two methods are special cased and limited to symmetric geometries, while the last one is for general cases. In this work, the PBCs integrating the uniform strain condition are applied for symmetrical BCC models.

For BCC lattice unit cell, as shown in Figure 1, the equivalent configuration is a cube consisting 3 pairs of opposite surfaces, noted as $\left\{A_i - A_i^{'}\right\}, i = 1, 2, 3$. PBCs are applied on corresponding surfaces of $A_1 - A_1^{'}$, $A_2 - A_2^{'}$, and $A_3 - A_3^{'}$. The stress vectors on opposite directions have the magnitude but different signs. For a structure comprised of an enormous number of periodic cells and behaving in a homogenized form with the assumption of a homogenous body, the external displacement results in a E over the body. Due to the presence of heterogeneous resulting from voids within the lattice, a correlation $\boldsymbol{\varepsilon}^{\mathrm{per}}$ should be considered on the periodic boundaries and the microscopic strain ε can be regarded as the superposition of E and a fluctuating part $\boldsymbol{\varepsilon}^{\mathrm{per}}$, explained specifically as:

$$\begin{cases} \varepsilon = \mathbf{E} + \varepsilon^{\mathrm{per}}(x), \\ \boldsymbol{u} = \mathbf{E} \cdot x + u^{\mathrm{per}}(x), \end{cases} \tag{6}$$

where $\boldsymbol{u}$ and $u^{\mathrm{per}}(x)$ represent the corresponding displacement and correlation part according to $\boldsymbol{\varepsilon}$ and $\varepsilon^{\mathrm{per}}(x)$.

In this work, the PBCs with the uniform strain condition (Voigt's bound) is applied on the lattice cell that satisfies the uniform strain rate within the lattice RVE. In this context, considering the symmetric geometry of the BCC lattice, the uniform strain E is imposed on ∂V with the following formulations:

$$\begin{cases} div\boldsymbol{\sigma}^{\boldsymbol{E}} = 0, \text{ in } V, \\ \langle \boldsymbol{\varepsilon} \rangle = \mathrm{E}, \\ \boldsymbol{\sigma}^{\boldsymbol{E}} = \boldsymbol{d} : \mathrm{E}, \\ \sigma \cdot \boldsymbol{n}, \text{ anti} - \text{periodic on } \partial V, \\ \boldsymbol{\varepsilon}^{\mathrm{per}} = 0, \\ \boldsymbol{u}^{\mathrm{per}}, \text{periodic on on } \partial V. \end{cases} \tag{7}$$

Then, the general boundary conditions are applied with:

$$\begin{cases} u_i + u_i^{'} = U_i^0, \\ u_i = 0, \\ u_i^{'} = U_i^0, \end{cases} \tag{8}$$

where U_i^0 represents the global displacement of the RVE.

Based on Voigt's bound-integrated PBCs, the uniform strain approach is adopted on one hand so that the uniform displacement restricts the deformation of the RVE. On the other hand, the conditions impose the constraints on both stress and strain fields, which results in stress and geometrical compatibility of the RVEs.

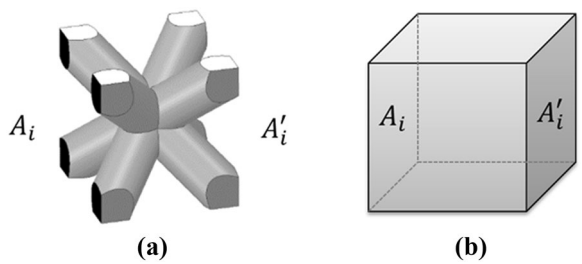

Figure 1 Periodic boundary condition: (**a**) Lattice unit cell, (**b**) Equivalent lattice unit

3 Nickel Metal Coating

3.1 Coating Process

Metallic coating treatment for 3D printed resin lattice structure was studied by a research team from Southeast University [32, 33]. Metallic coating is deposited on the surface of test sample via electroless plating process which includes four major steps [32]: (1) etching, (2) sensitization/activation, (3) acceleration, and (4) plating. The preparation of coated lattices was carried out as follows: test samples were first ultrasonically cleaned in isopropanol (C_3H_8O), and then immersed in strong $KMnO_4$ etchant for roughening the sample surface. After rinsing with deionized water (DI) water, the samples were sensitized/activated by dipping into a Pd/Sn colloidal catalyst solution. Then, samples

were submerged in acceleration solution for releasing Pd elementary particles. After thoroughly rinsing with DI water, the samples were immersed in alkaline nickel bath for metal plating.

3.2 Numerical Model of Coating

The coating thickness is measured in micrometer, usually in the range of (0, 50 μm), which is far thinner than the rod thickness of the lattice unit. The surface coating was modeled with the one-layer element named the Shell281 on the top of the matrix with the assumed transverse shear stiffness $E_{trans} = kGh$. Specifically, parameters of k, G, and h represent the shear-correction factor, shear modulus, and the thickness of the coating film, respectively.

Following this method, the coating film can be discretized by Shell281 elements with three stiffness behaviors: stress evaluation only (coating elements have no stiffness contribution to the model), membrane, and integration of membrane and bending. A drawback of this type of finite element modeling is lacking the possibility to study solid-surface interaction. However, simplicity and ease of modeling concerning both linear elasticity and nonlinear material assumptions is an advantage. On the other hand, surface-element-based modeling can eliminate huge numbers of discretized elements compared with hybrid solid elements.

4 Multiscale Evaluation Results

4.1 Finite Element Modelling and Material Preparation

The 3×4×15 BCC lattice model and coated lattice RVE is established at global and micro/mesoscopic scales, as shown in Figure 2(a), (b), respectively. The dimension of the lattice cell is 3 mm×3 mm×3 mm. η is the volume fraction of the lattice cell, which can be determined as:

$$\eta\% = \frac{V_{solid}}{V_{\text{cube}}}, \tag{9}$$

which reveals that η has the positive correlation with strut diameter (d) of the lattice. Considering the impact of d on the E of the metal-coated lattice structures, lattice cell models with three different d and corresponding η are listed in Table 1.

The lattice base is meshed by tetrahedron elements, while its coating film is meshed by Shell281 with three assumed stiffness behaviors as mentioned previously. The precision and effectiveness of these three proposed stiffness behaviors are also further assessed through numerical simulation and experiments. To determine the material properties of printed resin matrix, five dog-bone resin specimens were produced by SLA, as shown in Figure 3(a). The samples were printed by Formlabs2, with 45° printing orientation, adding the thickness up to 0.05 mm and exposing to air for one week. Then, specimens were subject to in-situ tensile tests by the Instron 5982 series extensometer with the stretching rate of 2 mm/min. Subsequently, it can be seen in Figure 3(b) that an adequate number of 3×4×15 lattice structures made of pure resin were manufactures through 3D printing-based additive manufacturing technology. After the coating processes, all lattice samples were coated with nickel films, as shown in Figure 3(c).

Due to the same standard manufacturing processes of nickel coating film stated in Ref. [34], the material properties of coating film for numerical simulation are selected accordingly. Hence, the material properties

Table 1 Lattice unit cells with different values of d

Lattice cell			
d(mm)	0.5	1.0	1.5
η(%)	12.85	42.32	67.73

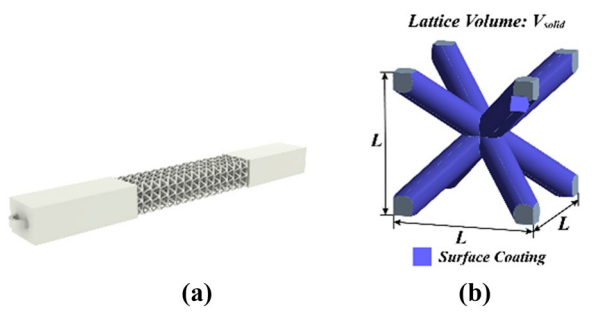

Figure 2 BCC-like lattice structure modeling at (**a**) global level and (**b**) RVE level

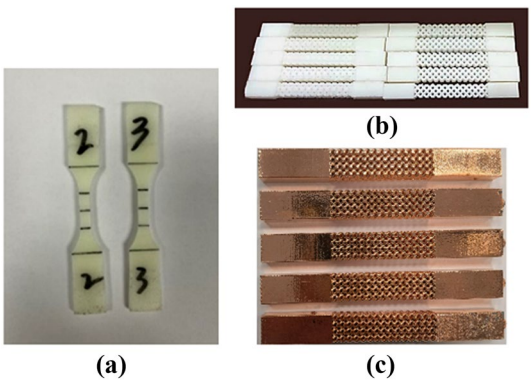

Figure 3 Experiment procedures with (**a**) resin dog-bone samples for material definition, (**b**) 3D printed lattice structure samples, and (**c**) coated lattice samples

Table 2 Material properties of base matrix and coating film

	Young's modulus (GPa)	Poisson's ratio υ	Density (kg/m^3)
Resin[1]	2.46	0.3	1100
Coating[2]	50	0.28	8500

Note: [1] Photosensitive resin DSM Somos 14120 from Xiamen Jiecheng 3D Technology; [2] Nickel alloy [34]

Table 3 E comparison between the benchmark and the proposed RVE-scale evaluation

Result source	Material benchmark	Homogenization-based method
E (GPa)	2.46	2.46

of the base matrix and nickel film are obtained and described in Table 2.

4.2 Validation of Numerical Modeling

To verify the proposed numerical evaluation approach, the printed pure lattice matrix without coating were analyzed.

4.2.1 Special Case: Solid Cube with Homogenous Material

A homogeneous lattice cube made of pure resin was first studied under the proposed Voigt's bound-integrated PBCs, E was accordingly evaluated, as shown in Table 3. Excellent matching is achieved between the initial material property and the homogenization-based method. Here, exact material properties of the base resin set in ANSYS Workbench 2020 R2 are based on Table 2. Considering the magnitude of d, the element size is set as 0.25 mm.

4.2.2 Literature Case of Metal Lattice Unit without Coating

The proposed PBC-based homogenization was secondly validated through a reference case by Refai [35]. A pure metal BCC lattice cell with parametrized d were studied for numerical evaluation of E. The material properties are selected accordingly as those in Ref. [35]. Under the proposed boundary conditions and uniaxial displacement δ=0.01 mm in x direction, the stress distribution and displacement contours of single lattice cell and the stress contour of the global structure were illustrated in Figure 4 and Figure 5, respectively. Obviously, good compatibilities of the displacement field within lattice cell and stress fields in global structure scale guarantee the rationality of the proposed method.

Based on the comparison between the obtained E by author and the reference, as indicated in Figure 6,

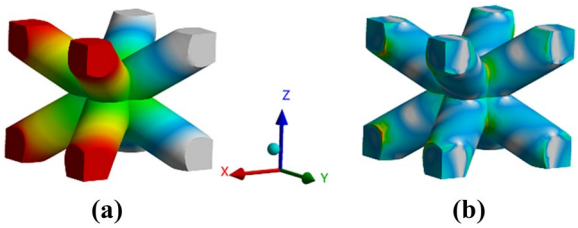

Figure 4 Result contours of the lattice unit with (**a**) stress field, and (**b**) transverse displacement

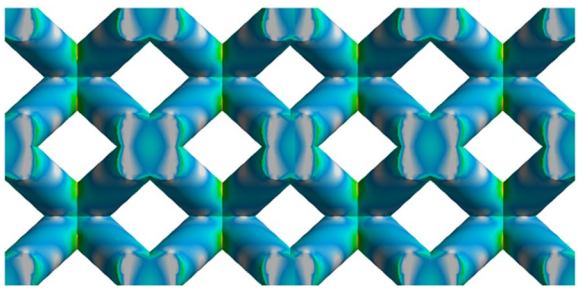

Figure 5 Stress field from the global perspective

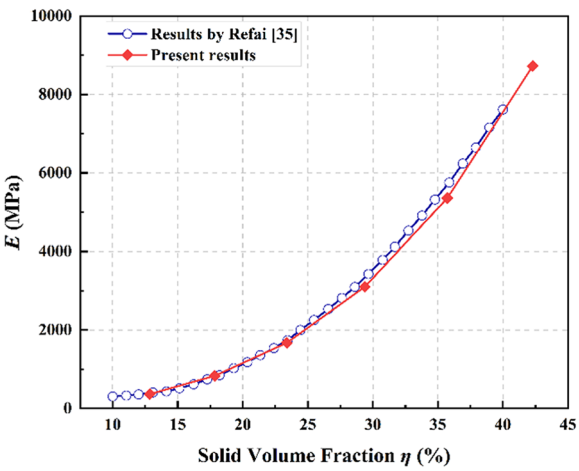

Figure 6 Comparison of E for BCC lattice RVE with parametrized d

an acceptable agreement is reached for the proposed homogenization-based methods. Thus, for lattice structures, the simple homogenization method using volumetric averaging of stress has probably led to the relative larger discrepancy due to a non-homogeneous mass moment of inertia attributing from a non-uniform spread of internal voids. According to the aforementioned deduction, RVE-based evaluation of the structural mechanical property following Eq. (5) is adopted for following numerical studies.

4.2.3 Experimental Validation

With pure polymer resin and nickel-coated lattices, the validation of the proposed method is thirdly carried out by the comparison of E obtained by RVE-scale-based numerical anticipation and structure-scale-based experiments. Here, the numerical model of the lattice cell and 3×4×15 lattice samples with d of 1 mm and 1.5 mm are utilized. As the output of tensile tests, stress-strain relationships of global lattice samples can be acquired, as shown in Figure 7(a), (b). Subsequently, E from numerical prediction is compared with its experimental counterpart, as indicated in Figure 7(c). The histograms correspond to the numerical result, and the error bars colored in red refers to the range of experimental results.

The (min, max) errors of numerical modeling with respect to experiments are achieved (3.22%, 9.55%) and (0.38, 5.78%) for resin BCC lattice structure with d of 1 mm and 1.5 mm, respectively. That is to say, the experimental data of lattice samples with d of 1.5 mm is smaller than that with d of 1 mm, which is probably affected by the washing treatment. The lattice samples with d of 1.5 mm were immerged in the cleaning fluid longer time to remove the supporting materials of the voids.

Moreover, E of nickel-coated lattice structures are also evaluated through micro/mesoscopic lattice numerical RVE with 3×3×3 lattice cells and macroscopic experiments with samples of d=0.5 mm and coating thickness (T)=5 μm, as shown in Figure 8. For Shell281 element with the stiffness behavior of stress evaluation only, it ignores the impact of T. This mainly explains why the considerable disparity is witnessed between experiments and simulations. However, the numerical accuracy is significantly improved for the two coating models with the stiffness behavior of membrane and bending. Therefore, it is worth noting that for accurate E assessment of the nickel-coated lattice structure, numerical elements of the nickel coating film should comprise the stiffness behavior of membrane and bending.

4.3 Stability of RVE Definition

An RVE is defined appropriately when its homogenized properties are size independent. For the lattice structure made of uniform cells, if the smallest repeatable unit can represent the homogenized material properties, the same volume monolithic structure (rectangular solid cube) should have the same properties. No matter it was expanded to other dimensions, the effective properties should be stable. Here, RVEs comprising three different numbers of lattice cells (1×1×1, 2×2×2, 3×3×3, and 4×4×4) are selected to evaluate E under the condition that d is fixed to 0.5 mm, 1.0 mm, and 1.5 mm and T varies from 0 to 25 μm.

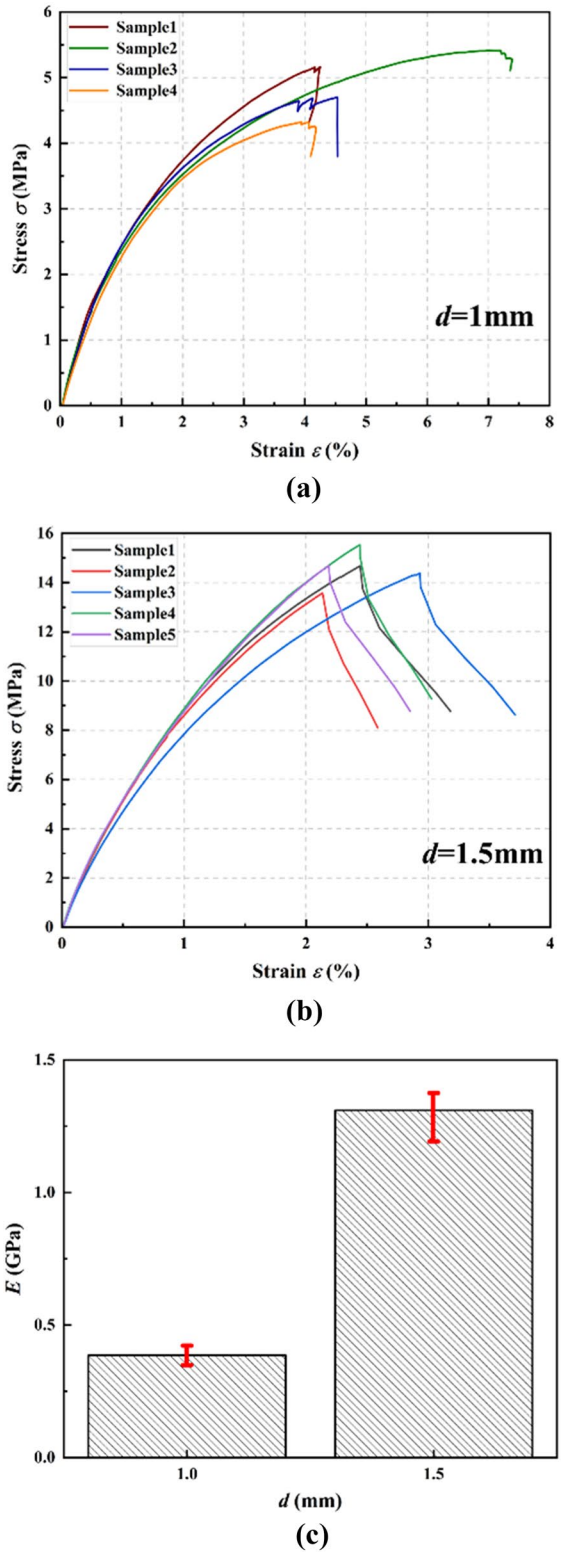

Figure 7 Method validation by E comparison of the resin lattice between numerical and experiment results

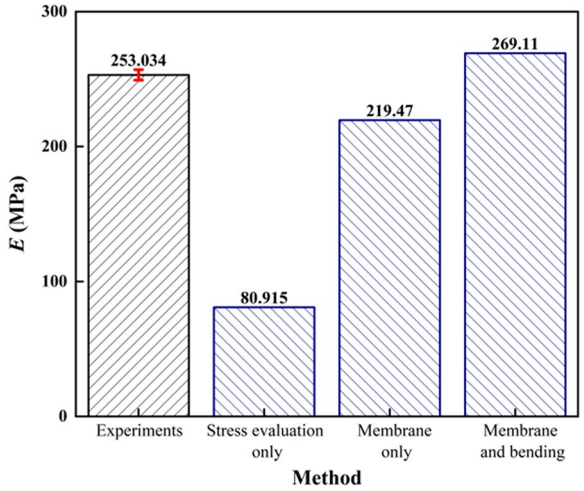

Figure 8 Comparison of E between numerical simulations based on diverse coating modeling methods and experiments

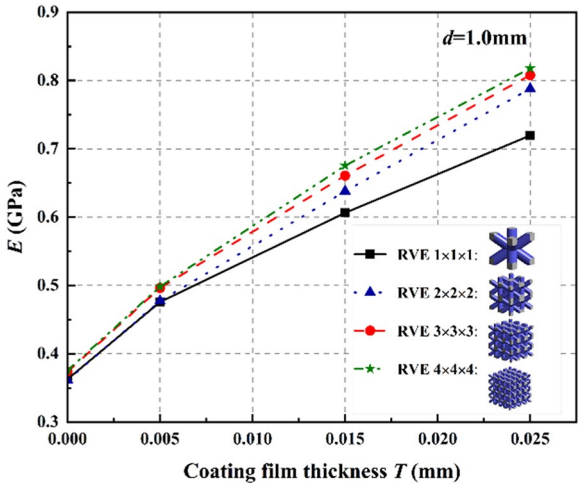

Figure 10 E variation of nickel-coated BCC lattice RVE concerning T with different number of cells (d = 1.0 mm)

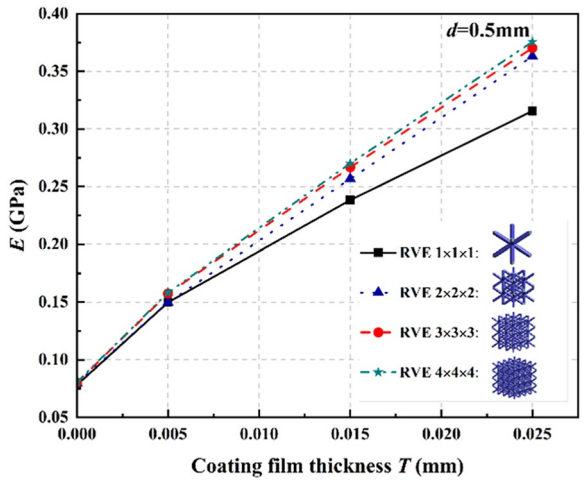

Figure 9 E variation of nickel-coated BCC lattice RVE concerning T with different number of cells (d = 0.5 mm)

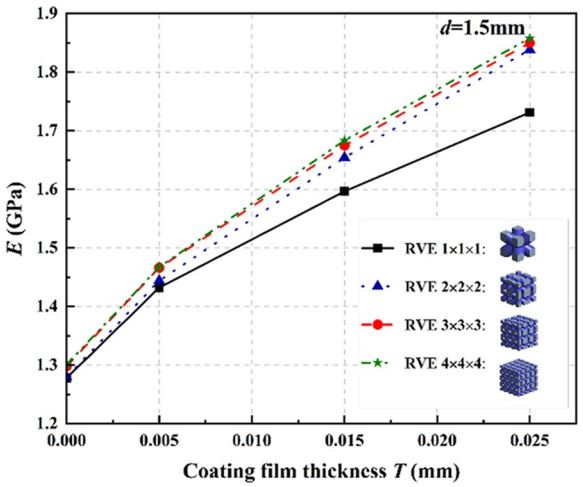

Figure 11 E variation of nickel-coated BCC lattice RVE concerning T with different number of cells (d = 1.5mm)

It can be observed from Figures 9, 10, 11 that homogenized material properties based on RVE tend to convergence when RVE size exceeds 2×2×2. In contrast, the property derived from RVE with a single cell has a relatively large discrepancy with the multiple ones. Therefore, compared with the conventional method of defining the minimal repeatable cell as the RVE of traditional composite materials, it can be concluded that for lattice structures, E evaluated from RVE with the multi-cell size should be more stable than from the RVE with the single cell. For coated BCC lattice structures that this work focuses on, the appropriate RVE size can be selected as 2×2×2 or 3×3×3 to achieve precise evaluations of the material properties.

4.4 Influence of the Strut Diameter and Coating Thickness

Although the impact of d on structural E was studied as a crucial parameter on lattice structure in the previous study [14], the variation of E concerning d is studied for the coated lattice structure at the RVE level for the first time. As shown in Figure 12, both positive contributions are made to E by d and T of the nickel-coated BCC lattice structure. However, d owns much larger sensitivity (75.90%) to E than T (25.78%), which means that the impact of d tends to be more aggressive. It provides an

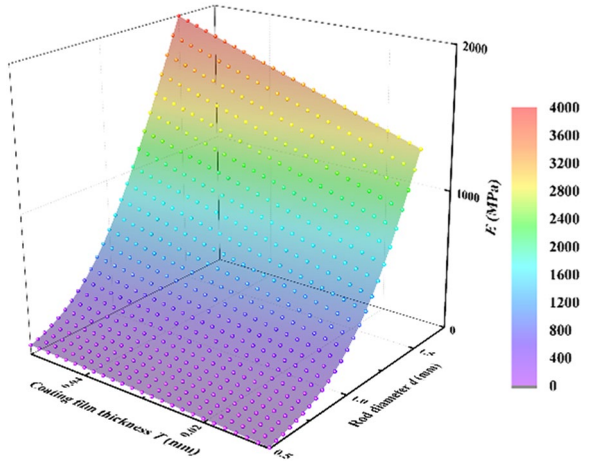

Figure 12 Overall impacts of d and T on E with the corresponding response surface

efficient way to improve coated BCC lattices' mechanical response in the structural design.

Based on the 2×2×2 lattice RVE, the influences of d and T on E are indicated in Figure 13. Apparently, E increases with the increase of either d or T, and vice versa. Moreover, the significant soar of E with increased d reasonably guarantees the effectiveness of sensitivity results in Figure 12.

4.5 Stiffness to Weight of Nickel-coated Lattices

It is obvious that the coated film will increase the elastic stiffness and strength of the entire lattice structures compared with lattices made of pure resin owing to the density of the coating material is much higher than the base matrix. Therefore, the overall performance of stiffness-to-weight ratio, also known as specific modulus e is studied. e can be calculated as follows:

$$e = \frac{E}{\rho}, \tag{10}$$

where ρ is the average density defined as total mass over the lattice cubic volume. High specific modulus materials may have wide applications where minimum weight is required.

As shown in Figure 14, e of lattice RVEs with the nickel film increases remarkably compared with that without coating. However, the increasing rate tends to slow down with the rising d. It reveals that the metal coating film has a more obvious contribution to the mechanical property improvement of the BCC lattice structure with smaller struts. However, when T increased linearly, e is not improved monotonously. Therefore, there should be an optimal T for the maximum stiffness-weight-ratio of the coated lattice structure. For the BCC nickel-coated lattice structure in this work, 15 μm could be a recommend value.

5 Conclusions

A multiscale evaluation of mechanical properties for nickel-coated BCC lattice structures is well studied in this work. Some conclusions can be drawn:

(1) When performing the homogenization analysis of coated BCC lattice, compared to the volume averaged stress, utilizing the reaction force yields a more accurate prediction.
(2) For lattice homogenization, RVE with multiple coated lattice cells combined with stiffness behavior of membrane and bending in coating modeling should be selected for more precise numerical evaluation.

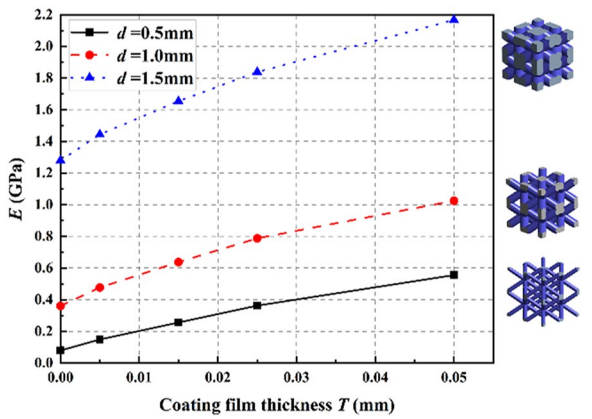

Figure 13 E evaluation of the nickel-coated BCC lattice with different d and T based on the 2×2×2 sized RVE

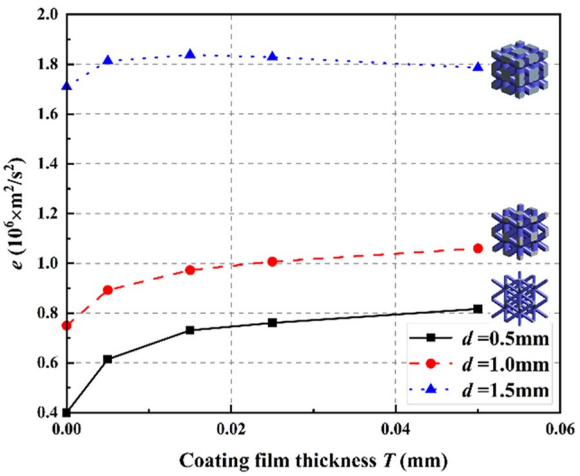

Figure 14 The e variation of nickel-coated lattices with d and T based on 2×2×2 sized RVE

(3) The increase of volume fraction, also represented by the strut diameter, has a big impact on the equivalent Young's modulus and specific modulus of the coated lattices.
(4) The coating film may remarkably increase the stiffness and specific modulus of the coated lattice structures. However, there should be an optimal coating thickness for the maximum structural stiffness-weight-ratio.

Acknowledgements
Not applicable.

Authors' Contributions
LW was in charge of conceptualization, methodology, software, writing-original draft; LH was in charge of material preparation, experiment launching, data processing; XW assisted with conceptualization, methodology, and writing editing; Sina Soleimanian was in charge of literature review, writing editing; YY was in charge of experiment supervision and data processing. MC led the supervision, writing-review & editing, and funding acquisition; GC was in charge of validation, writing–review & editing, and funding acquisition; JL was responsible for writing–review & editing, and funding acquisition. All authors read and approved the final manuscript.

Authors' Information
Lizhe Wang born in 1991, is currently a PhD candidate at *Xi'an Jiaotong-Liverpool University, China* and *University of Liverpool, UK*. He received his master degree in mechanical engineering.
Liu He born in 2000, is currently a MSc candidate at *Southeast University, China*. She received her bachelor degree in electronic science and technology.
Xiang Wang born in 1990, graduated from *Xi'an Jiaotong-Liverpool University, China* and he received his doctor degree in civil engineering.
Sina Soleimanian born in 1991, is graduated from *Xi'an Jiaotong-Liverpool University, China* and *University of Liverpool, UK* with the master degree and now he is working at Iran.
Yanqing Yu born in 1995, is currently a MSc candidate at *Southeast University, China*. She received her bachelor degree in electronic science and technology.
Geng Chen born in 1985, is currently a professor at *Beijing Jiaotong University, China*.
Ji Li born in 1983, is currently an associate professor at *Southeast University, China*.
Min Chen born in 1981, is currently an senior associate professor at *Xi'an Jiaotong-Liverpool University, China*.

Funding
Supported by National Natural Science Foundation of China (Grant Nos. 61974025, 61504024), National International Science and Technology Cooperation Base on Railway Vehicle Operation Engineering of Beijing Jiaotong University (Grant Nos. BMRV21KF07, BMRV20KF03) and XJTLU Research Development Fund of China (Grant Nos. RDF-17-02-44, RDF-SP-122).

Data availability
The datasets generated during and/or analysed during the current study are available from the corresponding author on reasonable request.

Declarations

Competing Interests
The authors declare no competing financial interests.

Received: 29 May 2023 Revised: 29 May 2023 Accepted: 25 June 2023
Published online: 12 September 2023

References

[1] S Soleimanian, A Davar, R Azarafza, et al. Theoretical, numerical, and experimental analyses of free vibrations of glass fiber reinforced polymer plates with central cutouts and free boundaries. *Mechanics of Advanced Composite Structures*, 2018, 5: 67-74.
[2] M Azhari, A R Shahidi, M M Saadatpour. Local and post local buckling of stepped and perforated thin plates. *Applied Mathematical Modelling*, 2005, 29: 633-652.
[3] H Takabatake. Static analysis of elastic plates with voids. *International Journal of Solids and Structures*, 1991, 28: 179-196.
[4] R M Gorguluarslan, U N Gandhi, R Mandapati, et al. Design and fabrication of periodic lattice-based cellular structures. *Computer-Aided Design and Applications*, 2016, 13: 50-62.
[5] D Fabris, J Mesquita-Guimarães, P Pinto, et al. Mechanical properties of zirconia periodic open cellular structures. *Ceramics International*, 2019, 45: 15799-15806.
[6] T D Ngo, A Kashani, G Imbalzano, et al. Additive manufacturing (3D printing): A review of materials, methods, applications and challenges. *Composites Part B: Engineering*, 2018, 143: 172-196.
[7] M Matthew, M Jurg, M Leary, et al. Programmatic lattice generation for additive manufacture. *Procedia Technology*, 2015, 20: 178-184.
[8] F Tamburrino, S Graziosi, M Bordegoni. The design process of additively manufactured mesoscale lattice structures: A review. *J. Comput. Inf. Sci. Eng.*, 2018, 18: 1-16.
[9] C Yanhong C, Z Weimin, W Shiwen, et al. Investigation of FE model size definition for surface coating application CDM-based constitutive model. *Chin. J. Mech. Eng.*, 2012, 25(5): 860–867.
[10] M Jimenez, S Duquesne, S Bourbigot. Intumescent fire protective coating: toward a better understanding of their mechanism of action. *Thermochim Acta*, 2006, 449: 16-26.
[11] Y Kojima, T Aizawa, S Kamado. Structure and corrosion behavior of conversion coatings on magnesium alloys. *Umehara-2000-Mat Sci Forum*, 2000: 273-282.
[12] C T Kao, C C Lin, Y W Chen, et al. Poly (dopamine) coating of 3D printed poly (lactic acid) scaffolds for bone tissue engineering. *Materials Science and Engineering C*, 2015, 56: 165-173.
[13] R Xiao, X Feng, R Fan, et al. 3D printing of titanium-coated gradient composite lattices for lightweight mandibular prosthesis. *Composites Part B: Engineering*, 2020, 193: 108057.
[14] J Song, L Gao, K Cao, et al. Metal-coated hybrid meso-lattice composites and their mechanical characterizations. *Composite Structures*, 2018, 203: 750-763.
[15] K B Yilmaz, I Çömez, M A Güler, et al. Analytical and finite element solution of the sliding frictional contact problem for a homogeneous orthotropic coating-isotropic substrate system. *ZAMM-Journal of Applied Mathematics and Mechanics/Zeitschrift für Angewandte Mathematik und Mechanik*, 2019, 99: e201800117.
[16] R Jahedi, S Adibnazari, G H Farrahi. Performance analysis of functionally graded coatings in contact with cylindrical rollers. *Advances in Mechanical Engineering*, 2015, 7:456848.
[17] B Sobol, A Soloviev, A Krasnoschekov. The transverse crack problem for elastic bodies stiffened by thin elastic coating. *ZAMM-Journal of Applied Mathematics and Mechanics/Zeitschrift für Angewandte Mathematik und Mechanik*, 2015, 95: 1302-1314.
[18] G Zhang, C He, B Wu, et al. Evaluating local elasticity of the metal nanofilms quantitatively based on referencing approach of atomic force acoustic microscopy. *Chin. J. Mech. Eng.*, 2012, 25(6): 1281–1286.
[19] E Ptochos, G Labeas. Elastic modulus and Poisson's ratio determination of micro-lattice cellular structures by analytical, numerical and homogenisation methods. *Journal of Sandwich Structures and Materials*, 2012, 14: 597-626.
[20] S Kurukuri. A review of homogenization techniques for heterogeneous materials. *Analysis*, 2004, 46.
[21] C Li, L Chen, L Qiao. RVE based numerical evaluation on effective mechanical properties of composite with randomly distributed multiphase inclusions. *Advanced Materials Research*, 2012, 383-390: 931-934.
[22] M Ostoja-Starzewski. Material spatial randomness: From statistical to representative volume element. *Probabilistic Engineering Mechanics*, 2006, 21: 112-132.
[23] N Carrere, R Valle, T Bretheau, et al. Multiscale analysis of the transverse properties of Ti-based matrix composites reinforced by SiC fibres: From

the grain scale to the macroscopic scale. *International Journal of Plasticity*, 2004, 20: 783-810.
[24] K Okomori, T Enomae, F Onabe. Evaluation and control of coated paper stiffness. *Japan Tappi Journal*, 1999: 121-132.
[25] H W Ng, Z Gan. A finite element analysis technique for predicting as-sprayed residual stresses generated by the plasma spray coating process. *Finite Elements in Analysis and Design*, 2005, 41: 1235-1254.
[26] I Bencheikh, F Bilteryst, M Nouari. Modelling of the thermomechanical behaviour of coated structures using single and multi-level-set techniques coupled with the eXtended Finite Element Method. *Finite Elements in Analysis and Design*, 2017, 134: 68-81.
[27] P M Dixit, S D Uday. *Plasticity fundamentals and applications*. CRC Press, 2015.
[28] I T Zohdi, P Wiggers. *An introduction to computational micromechanics*. Springer Science & Business Media, 2008.
[29] S Xin, L Zhang, M Chen, et al. Understanding influence of micro pores on strengths of LMDed AlSi10Mg material using a direct method based statistical multiscale framework. *Mater. Des.*, 2022, 214: 110409.
[30] Y K Khdir, T Kanit, F Zaïri, et al. Computational homogenization of plastic porous media with two populations of voids. *Materials Science and Engineering A*, 2014, 597: 324-330.
[31] M Chen, A Hachemi. Progress in plastic design of composites. In: *Direct methods for limit states in structures and materials.* Springer, 2014: 119-138.
[32] J Li, Y Wang, G Xiang, et al. Hybrid additive manufacturing method for selective plating of freeform circuitry on 3D printed plastic structure. *Advanced Materials Technologies*, 2019, 4: 1-10.
[33] J Li, Y Wang, P Wang, et al. Rapid production of customized 3D electronics via hybrid additive manufacturing technology. *Proceedings - Electronic Components and Technology Conference*, 2019: 135-140.
[34] T Sanderson. Measuring the elastic moduli of electroless nickel-phosphorus deposits. *Plating and Surface Finishing*, 2005, 92: 39-43.
[35] K Refai, M Montemurro, C Brugger, et al. Determination of the effective elastic properties of titanium lattice structures. *Mechanics of Advanced Materials and Structures*, 2020, 27: 1966-1982.